Tree ring–based seven-century drought records for the Western Himalaya, India

Ram R. Yadav[1]

[1]   The paucity of available instrumental climate records in cold and arid regions of the western Himalaya, India, hampers our understanding of the long-term variability of regional droughts, which seriously affect the agrarian economy of the region. Using ring width chronologies of *Cedrus deodara* and *Pinus gerardiana* together from a network of moisture-stressed sites, Palmer Drought Severity Index values for October–May back to 1310 A.D. were developed. The twentieth century features dominant decadal-scale pluvial phases (1981–1995, 1952–1968, and 1918–1934) as compared to the severe droughts in the early seventeenth century (1617–1640) as well as late fifteenth to early sixteenth (1491–1526) centuries. The drought anomalies are positively (negatively) associated with central Pacific (Indo-Pacific Warm Pool) sea surface temperature anomalies. However, non-stationarity in such relationships appears to be the major riddle in the predictability of long-term droughts much needed for the sustainable development of the ecologically sensitive region of the Himalayas.

Citation: Yadav, R. R. (2013), Tree ring–based seven-century drought records for the Western Himalaya, India, *J. Geophys. Res. Atmos.*, *118*, 4318–4325, doi:10.1002/jgrd.50265.

1.   Introduction

[2]   The western Himalayan region, north of the Pir Panjal Range, India, is semi-arid to arid and usually experiences little summer monsoon rain. Instrumental weather records available from Purbani, a cold and arid region in Kinnaur, Himachal Pradesh, show that June–September precipitation represents around 20% of the annual total (~613 mm), when the cis-Himalayan region receives plenty of summer monsoon rains. Most of the socioeconomic activities in the region are therefore largely dependent on winter and spring precipitation occurring largely due to eastward propagating mid-latitude cyclones from the Atlantic Ocean and the Mediterranean Sea [*Martyn*, 1992]. Any failure or weakening of precipitation during these seasons causes drought, constraining socioeconomic development. The recent droughts of 1999–2001 were widespread over the Southwest central Asia region [*Hoerling and Kumar*, 2003] and seriously affected agricultural production in Kinnaur in the western Himalaya [*Himachal Pradesh Development Report*, 2005]. Understanding the recurrence behavior and magnitude of such droughts in the long-term context is required to adopt drought mitigation contingency plans. However, the paucity of weather records from high-elevation cold and arid regions hampers our efforts toward this end. The utility of weather records available from lower elevations is seriously limited due to the high spatial variability of climate under dominant orographic forcing [*Yadav*, 2007], warranting the need to develop high-resolution proxy climate records from different orographically separated basins in the Himalayas.

[3]   Many old-age trees growing in semi-arid to arid regions of the high-elevation western Himalaya provide valuable high-resolution archives of climate. It has been observed that the growth of trees in such regions, irrespective of species, is usually favored by cool, wet springs [*Yadav and Park*, 2000; *Singh and Yadav*, 2005; *Singh et al.*, 2009; *Yadav*, 2011a, b]. The tree ring chronologies developed from different ecological settings in the western Himalaya until now have been largely used to develop precipitation and temperature reconstructions [*Hughes*, 2001; *Yadav and Park*, 2000; *Singh and Yadav*, 2005; *Singh et al.*, 2009; *Yadav*, 2011a, b; *Yadav et al.*, 2011]. The present study is the first attempt to develop drought indices (Palmer Drought Severity Index, PDSI) [*Dai et al.*, 2004] for the high-elevation cold and arid regions of the western Himalaya using ring width chronologies of Himalayan cedar (*Cedrus deodara* (Roxb.)) and Neoza pine (*Pinus gerardiana* Wall. ex Lamb.). The strong similarity in the growth patterns of these two species, occurring in similar ecological settings, provided the basis for using them together. The reconstructed PDSI series have been used to analyze variability in droughts and their association with large-scale sea surface temperature (SST) anomalies over the Indo-Pacific region in a long-term perspective.

────────

Additional supporting information may be found in the online version of this article.

[1]Birbal Sahni Institute of Palaeobotany, Lucknow, India.

Corresponding author: R. R. Yadav, Birbal Sahni Institute of Palaeobotany, 53 University Road, Lucknow 226007, India. (rryadav2000@gmail.com)

2. Materials and Methods

2.1. Tree Ring Data

[4] The Himalayan cedar and Neoza pine trees in Kinnaur are found growing disjunctly on steep rocky slopes with very thin soil cover. Climatic signals in tree ring materials from such ecological settings are expected to be high as the growth ring sequences in them are least affected by stand dynamics. The potential of tree ring materials of Himalayan cedar and Neoza pine collected in summer 2005 from the drought-prone Kinnaur region was first established by Singh *et al.* [2009]. The growth patterns of these two species growing over homogeneous ecological settings are very similar, except that the missing rings are more frequent in Neoza pine (~4.1%) as compared to Himalayan cedar (~3.4%). To develop robust long-term precipitation records for this cold and arid region, the tree ring materials collected in 2005 were supplemented with Himalayan cedar samples collected afresh in summer 2006 from 10 more sites of ecologically homogeneous settings in Kinnaur. This updated tree ring data network, with a sum of 116 tree samples from 11 sites, was used to reconstruct spring (March–June) precipitation (1410–2005 A.D.) for this region using chronology developed through the regional curve standardization method [*Yadav*, 2011a]. The PDSI, a likely candidate most suited to describe meteorological drought over this cold and arid region of the western Himalaya, could not be developed using the above chronologies due to poor calibration statistics. Hence, toward this objective, the tree ring data network was further strengthened with the collection of a large number of tree ring samples of Himalayan cedar and Neoza pine in summer 2011. In all, tree ring samples of Himalayan cedar from 9 sites (a sum of 420 cores from 294 trees) and Neoza pine from 2 sites (a sum of 126 cores from 107 trees) (Figure 1) were used in the present study. Standard dendrochronological methods were adopted in the development of
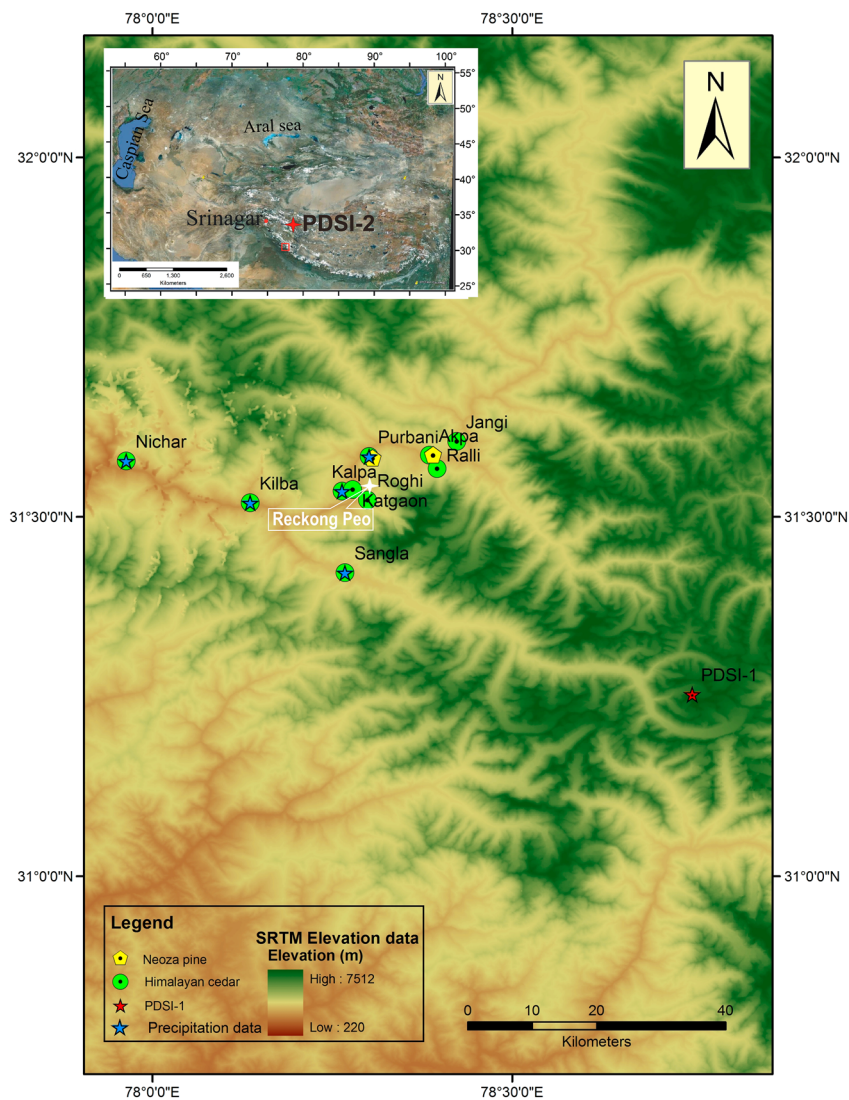
Figure 1. Map showing the locations of the tree ring sampling sites and meteorological stations used in this study. The red lined rectangle in the inset map representing the study area is again shown in magnified scale. The dotted fluorescent green circles, dotted yellow polygons, red stars, and blue stars represent Himalayan cedar, Neoza pine, PDSI grid 1, and PDSI grid 2, respectively. The PDSI grid 2 location and Srinagar meteorological station are indicated in the inset map.

tree ring chronologies from different sites (see Data and Methods in Auxiliary Materials, Table S1, and Figure S1). A cross-correlation analysis was performed to understand the relationships among the site and species chronologies. Strong correlations among the chronologies over the common period 1660–2005 (Table S2) showed common climate forcing affecting the growth of both species over all study sites.

2.2. Climate Data and Relationship With Tree Ring Chronologies

[5] No climate data are available from the high-elevation locations in the western Himalaya where we have been able to locate very old living trees still growing in healthy conditions. However, due to the presence of several hydropower projects on the Satluj River, precipitation data from the Kinnaur region are better recorded at various locations in the river catchment area. Precipitation in Kinnaur predominantly occurs in December–May, and summers are usually dry except in years of strong monsoon when stray showers occur. The precipitation records from five stations close to the sampling locations in the lower catchment of the Satluj River, which show good coherence [*Yadav*, 2011a], were used in this study (see Data and Methods in Auxiliary Materials, Tables S3 and S4). The monthly mean precipitation anomalies of all five stations were merged to prepare a regional mean series. This regional mean monthly precipitation series was used to study climate-growth relationships. As temperature records are not available from this area, data from the Srinagar station (34°08′N, 74°48′E, 1587 m asl; 1893–2010 A.D.), located in a nearly similar climatic regime as that prevailing over the tree ring sites, were used to understand their relationship with tree ring chronologies.

[6] To investigate the relationship between tree growth and climate variables, residual chronologies (nine of Himalayan cedar and two of Neoza pine) developed from different sites were cross-correlated with monthly precipitation and temperature variables from September of the previous growth year to August of the current year (Figures 2a and 2b). The monthly precipitation from September of the previous year to July of the current year showed a positive relationship. However, the correlations were highly significant during boreal spring (March–May; $p \leq 0.01$). The relationships with mean monthly temperature were found to be negative for the full dendrochronological year, with the strongest correlations again being in boreal spring (March–May; $p \leq 0.01$). The first principal component (PC#1) of the residual chronologies of 11 sites calculated for the common period 1660–2005 A.D. (accounting for 85% of the common variance) also revealed a similar relationship with monthly precipitation and temperature variables as noted for the individual chronologies. These findings revealed that the availability of soil moisture, a function of precipitation and temperature, is very important for tree growth at the studied sites. The chronologies were tested for relationships with PDSI, which is widely used as a measure of meteorological drought over land regions [*Dai et al.*, 2004]. The 2.5° × 2.5° gridded PDSI values were extracted from the Palmer Drought data set (http://www.cgd.ucar.edu/cas/catalog/climind/pdsi.html) for two grid points close to the tree ring sampling locations in the western Himalaya (31.25°N–78.75°E and 33.75°N–78.75°E; Figure 1). The PDSI values from 1949–2005 were taken for study as the meteorological data used in estimating the PDSI are commonly available for this period. The monthly PDSI values of both grid points showed a strong positive relationship with the respective site chronologies and PC#1. The robust relationship noted between PC#1 and October–May (OM) PDSI (Figure 2c) was taken to develop the reconstruction. Monthly PDSIs of two grid locations from OM were merged to prepare mean seasonal series for calibration and reconstruction.
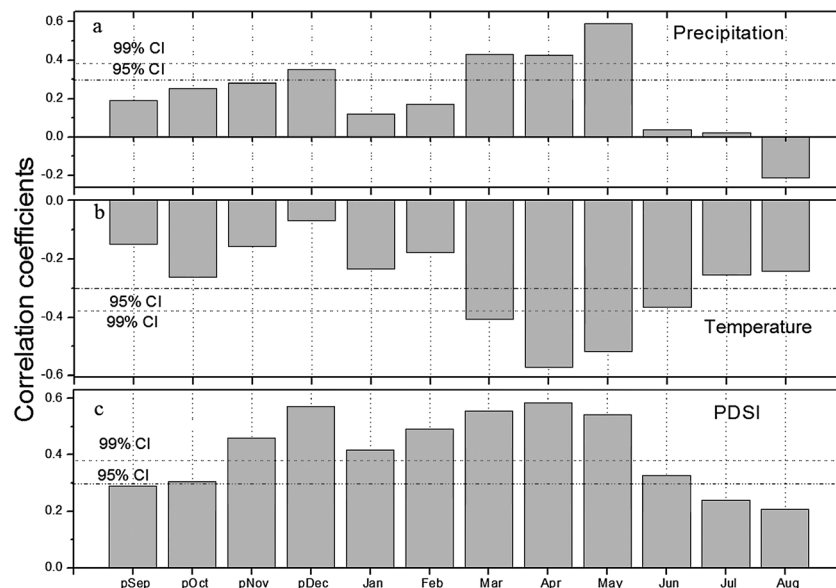
Figure 2. Correlation between PC#1 values of the residual version of the chronologies (Himalayan cedar and Neoza pine). (a) Monthly precipitation. (b) Mean monthly temperature series. (c) Mean monthly PDSI of the two grid points. Climate variables spanning from September of the previous year to August of the current year were used in correlations. The 95% and 99% confidence limits of the correlation are indicated by dotted lines.

2.3. Reconstruction of OM PDSI

[7] To obtain low-frequency variations in OM PDSI reconstruction, a PC regression (PCR) approach involving standard versions of the 11 site chronologies was used. For this predictor chronology variables (t0 and t + 1) were tested for their relationship with OM PDSI. The chronology variables showing a significant relationship (with significance level of 0.01 or better in two-tailed test) in the calibration period (1949–2005) were used in the PCR analysis. Only t0 chronology variables of the two species spread over all 11 homogeneous sites (Table S1) were selected for development of the reconstruction model. To optimize the reconstruction length, a nested approach [*Cook et al.*, 2003] was adapted. The split-period calibration-verification scheme using PDSI data from 1949–2005 in two subperiods, 1949–1977 and 1978–2005, was used to test the veracity of calibration models in reconstruction. Rigorous calibration and verification statistics, such as the reduction of error (RE), coefficient of efficiency (CE), Sign test, and Pearson correlation coefficient [*Fritts*, 1976; *Cook et al.*, 1999], were used to test the significance and reliability of the reconstruction (Table 1). Positive values of both the RE and the CE in verification periods denote statistical skill in the reconstruction. In this way, 10 reconstructions of different lengths using a varying number of predictor chronologies were developed. The nested reconstructions developed using the full-period (1949–2005) calibrations were spliced together to develop the final reconstruction extending from 1310 to 2005 A.D. However, in order to minimize the artifact associated with the changes in variance through time due to the decreasing number of predictors, the mean and standard deviation of each nested series were scaled to those of the most replicated nest (1660–2005) prior to averaging. The reconstructed mean PDSI series thus developed revealed close similarity and significant correlation with the mean observed OM PDSI series (r = 0.61, p < 0.0001; Figure 3).

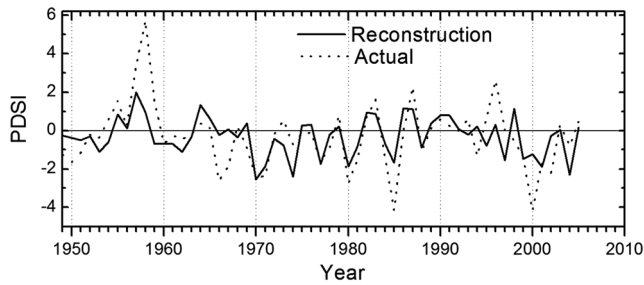## 3. Analysis of OM PDSI Reconstruction

[8] The OM PDSI reconstruction (1310–2005 A.D.) indicates strong interannual to multidecadal variations in droughts over the western Himalayan region (Figure 4). The reconstructed OM PDSI series is strongly correlated with a spring (MAMJ) precipitation reconstruction (r = 0.81; 1410–2005) developed earlier for this region using the predictor chronology of a single species (Himalayan cedar) [*Yadav*, 2011a]. However, it should be noted that both reconstructions are not completely independent as the OM PDSI reconstruction shares some of the Himalayan cedar tree ring data used in MAMJ precipitation reconstruction. The above two series plotted together revealed close similarity except in the early part of the fifteenth century when MAMJ precipitation values were lower. The lower values in MAMJ precipitation could have been caused by the use of a predictor chronology developed using the regional curve standardization method [*Yadav*, 2011a], which is known to preserve low-frequency variations [*Briffa et al.*, 1992; *Cook et al.*, 2000]. The reconstructed OM PDSI series showed a negative relationship with mean summer temperature (May–August) [*Yadav et al.*, 2011] developed for the

Table 1. Calibration and Verification Statistics[a] of Different Nests

| S. No. | Proxy Nests | Number of Series | Calibration | | Verification | | | | |
			Period	ar^2 (%)	Period	R	Sign test	RE	CE
1	1660–2005	11	1949–2005	36	1978–2005	0.668 (0.0001)	23$^+$/5$^-$ (0.0009)	0.390	0.369
			1949–1977	30	1949–1977	0.574 (0.0011)	16$^+$/13$^-$ (0.711)	0.274	0.263
			1978–2005	43					
2	1640–2005	10	1949–2005	35	1978–2005	0.667 (0.0001)	23$^+$/5$^-$ (0.0009)	0.392	0.370
			1949–1977	29	1949–1977	0.564 (0.0018)	16$^+$/13$^-$ (0.711)	0.267	0.244
			1978–2005	42					
3	1540–2005	9	1949–2005	36	1978–2005	0.664 (0.0001)	23$^+$/5$^-$ (0.0009)	0.390	0.369
			1949–1977	31	1949–1977	0.575 (0.0014)	16$^+$/13$^-$ (0.711)	0.282	0.259
			1978–2005	42					
4	1535–2005	8	1949–2005	36	1978–2005	0.657 (0.0001)	23$^+$/5$^-$ (0.0009)	0.383	0.362
			1949–1977	31	1949–1977	0.577 (0.0013)	16$^+$/13$^-$ (0.711)	0.287	0.265
			1978–2005	41					
5	1515–2005	7	1949–2005	36	1978–2005	0.660 (0.0001)	23$^+$/5$^-$ (0.0009)	0.386	0.365
			1949–1977	30	1949–1977	0.573 (0.0014)	16$^+$/13$^-$ (0.711)	0.280	0.257
			1978–2005	41					
6	1495–2005	6	1949–2005	37	1978–2005	0.656 (0.0001)	23$^+$/5$^-$ (0.0009)	0.390	0.369
			1949–1977	33	1949–1977	0.594 (0.0011)	16$^+$/13$^-$ (0.711)	0.315	0.293
			1978–2005	41					
7	1440–2005	5	1949–2005	37	1978–2005	0.656 (0.0001)	23$^+$/5$^-$ (0.0009)	0.377	0.356
			1949–1977	34	1949–1977	0.606 (0.0006)	16$^+$/13$^-$ (0.711)	0.317	0.295
			1978–2005	41					
8	1435–2005	4	1949–2005	38	1978–2005	0.645 (0.0002)	22$^+$/6$^-$ (0.0037)	0.369	0.347
			1949–1977	36	1949–1977	0.619 (0.0004)	16$^+$/13$^-$ (0.711)	0.340	0.319
			1978–2005	39					
9	1430–2005	3	1949–2005	37	1978–2005	0.639 (0.0003)	22$^+$/6$^-$ (0.0037)	0.380	0.359
			1949–1977	34	1949–1977	0.596 (0.0006)	16$^+$/13$^-$ (0.711)	0.333	0.316
			1978–2005	38					
10	1310–2005	2	1949–2005	32	1978–2005	0.617 (0.0004)	22$^+$/6$^-$ (0.0037)	0.367	0.345
			1949–1977	27	1949–1977	0.545 (0.0022)	18$^+$/11$^-$ (0.265)	0.287	0.264
			1978–2005	36					

[a]As described by *Fritts* [1976] and *Cook et al.* [1999].

Figure 3. Actual and reconstructed OM PDSI series plotted together for comparison. OM PDSI data for 1949–2005 were used in calibration.
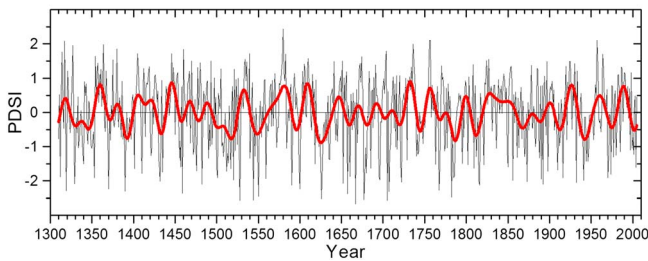

Figure 4. OM PDSI reconstruction (1310–2005 A.D.) for the western Himalaya overlaid with 20 year low-pass filtered version (thick line).

western Himalayan region (r = −0.17, p < 0.0007; 1310–2005), endorsing that wet (dry) winters are associated with cool (warm) ensuing summers. The present OM PDSI reconstruction was further compared with the Monsoon Asia Drought Atlas (MADA) June–August (JJA) PDSI reconstruction for the grid point 33.75°N and 78.75°E in the western Himalaya [*Cook et al.*, 2010] (Figure 5). The reconstructed OM PDSI was found to have a significant correlation with the MADA JJA PDSI (r = 0.20, p < 0.0001; 1310–2005). However, this relationship was found to be stronger in the latter part of the reconstruction (1800–1899: r = 0.55, p < 0.0001; 1900–2005: r = 0.45, p < 0.0001). It should be noted here that the present OM PDSI reconstruction is completely independent of MADA [*Cook et al.*, 2010] as they do not share any common tree ring data. Spatial correlation fields using the present reconstruction and regional gridded PDSI series revealed a strong positive association between droughts over the western Himalayan region and droughts in corresponding months over central Asia and Southwest Asia as well as negative correlations with moisture conditions over Southeast Asia (Figure 6).
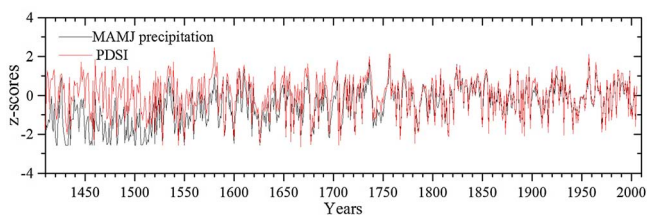
Figure 5. OM PDSI reconstruction plotted with MADA JJA PDSI reconstruction for the grid point 33.75°N and 78.75E in the western Himalaya [*Cook et al.*, 2010].
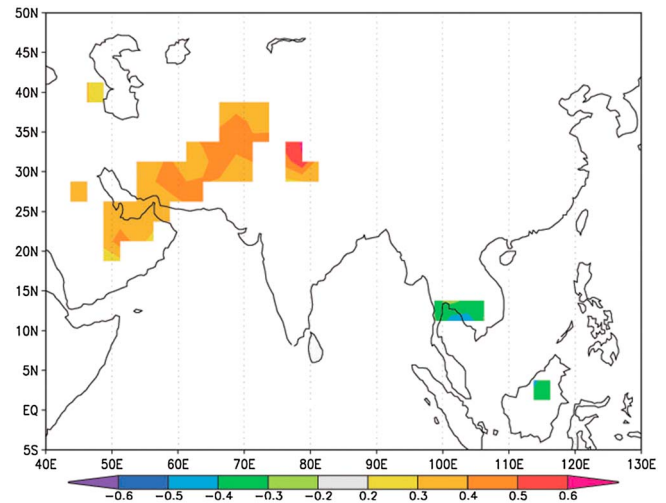
Figure 6. Spatial correlation between reconstructed OM PDSI and gridded PDSI of the corresponding months for 1950–2005. A strong positive relationship with drought over central Asia and Southwest Asia and a negative relationship with PDSI over Southeast Asia are noted. The picture was generated using the KNMI Climate Explorer program [http://climexp.knmi.nl; *Oldenborgh and Burgers*, 2005].

[9] The drought/pluvial regimes in the OM PDSI reconstruction were assessed on the basis of their duration (continuous years of negative/positive anomalies), magnitude (cumulative anomalies for a given number of years), and severity (ratio of magnitude and duration) [*Dracup et al.*, 1980]. Severe droughts occurred in successive years during 1677–1678 and 1815–1816, which also constituted part of the longer-term droughts from 1677–1682 and from 1812–1816, respectively. Other periods of extended droughts occurred in 1387–1397, 1617–1640, and 1740–1750. Extended pluvial phases in terms of magnitude occurred in 1354–1364, 1730–1739, and 1530–1538. To investigate the periods of longer-term droughts, 10 year and 20 year moving averages of the OM PDSI anomalies were calculated. The beginning of the drought/pluvial year was identified as the year when the moving average was negative/positive and the end period when the moving average returned to the opposite sign. The long-term drought/pluvial events recorded in the reconstruction are shown in Table 2. The OM PDSI reconstruction revealed long-term persistent droughts around 1617–1640 and 1491–1526, with the former period being the most severe in the context of the last seven centuries. However, contrary to the early sixteenth century droughts recorded in the present reconstruction, tree ring records from northern Karakoram, Pakistan, have shown an extended pluvial phase [*Treydte et al.*, 2006]. Such spatial heterogeneity in tree ring–based precipitation records warrants the development of a denser network of data from the orographically dissected Himalayan regions to better understand the variability in regional climate. The pluvial phases in the reconstruction indicated during the late sixteenth (1561–1590) and early nineteenth (1823–1857) centuries are coincident with the positive anomalies in MAMJ precipitation over the western Himalaya [*Yadav*, 2011a]. The early nineteenth century OM pluvial conditions are well corroborated by the record of glacier expansion in the Himalayas [*Fagan*, 2000]. Such an increased

Table 2. Dry and Wet Episodes Detected in 10 Year and 20 Year Running Means of the OM PDSI Reconstruction

	Dry				Wet		
Period	Severity (PDSI)	Duration (years)	Rank	Period	Severity (PDSI)	Duration (years)	Rank
Ten Year Mean							
1617–1635	−1.48	19	I	1354–1366	1.45	13	I
1777–1793	−1.18	17	II	1564–1585	1.25	22	II
1808–1819	−1.12	12	III	1726–1740	1.24	15	III
1385–1399	−1.11	15	IV	1604–1616	1.22	15	IV
1500–1528	−1.02	29	V	1529–1540	1.10	12	V
1427–1436	−1.00	10	VI	1981–1995	1.01	15	VI
Twenty Year Mean							
1617–1640	−1.52	24	I	1561–1590	1.33	30	I
1491–1526	−1.31	36	II	1823–1857	1.24	35	II
1935–1954	−1.09	20	III	1403–1423	1.02	21	III
1541–1560	−1.07	20	IV	1601–1616	1.01	16	IV
1768–1796	−1.04	29	V	1981–1996	0.96	16	V
1325–1349	−1.01	25	VI	1350–1374	0.92	25	VI
1862–1893	−0.72	32	VII	1439–1463	0.87	25	VII
1378–1402	−0.71	25	VIII	1917–1934	0.87	18	VIII
1803–1819	−0.69	17	IX	1721–1767	0.74	47	IX

wetness in the early nineteenth century over the western Himalaya could have also been responsible for the reduction in summer monsoon (June–September) rainfall over India [*Sontakke et al.*, 2008] through the mechanism of a dampened land-sea thermal gradient. The twentieth century experienced protracted droughts during 1935–1954; however, the severity of these droughts was subdued as compared to that of more severe droughts recorded in the early seventeenth and early sixteenth centuries. A drying trend in the western Himalaya in recent decades has begun following the 1981–1995 pluvial. In view of the increased hydrological demand due to the burgeoning population and intense agricultural activities on irrigated lands, the increasing droughts since 1996 might lead to serious economic constraints as compared to the economic impact of other historical droughts of similar magnitude.

[10] In order to understand the association between the OM PDSI anomalies over the western Himalayan region and large-scale SST [gridded HADISST global ocean surface temperature, monthly 1° area grids from 1870 to present, Hadley Centre, UK; *Rayner et al.*, 2003], spatial correlation fields were generated. The observed and reconstructed PDSI anomalies revealed that droughts over the western Himalayan region are positively associated with SSTs over the cool tongue of the Pacific and negatively associated with the Indo-Pacific Warm Pool (IPWP) region (Figure 7). In conformity with the above observations, it was found that the largest ENSO (El Niño) event of the twentieth century (1983) is associated with high OM precipitation over northwest India and droughts over Southeast Asia (Figure 8a). However, the La Niña event of 2000–2001 caused severe droughts over large parts of central Asia and Southwest Asia as well as pluvials over Southeast Asia (Figure 8b). Wet season precipitation (November–April) records available from Patseo (1983–2010) in Lahaul, a cold desert region in the western Himalaya, also indicate reduced precipitation in 1999–2001 coinciding with an extended La Niña event and a warm IPWP region. To test this relationship with SSTs in a longer-term context, correlation fields were generated for different time windows using the observed and reconstructed OM PDSIs. The correlation field results revealed a non-stationary relationship between OM PDSI and large-scale SSTs over the Indo-Pacific region. The relationship was found to be non-existent during
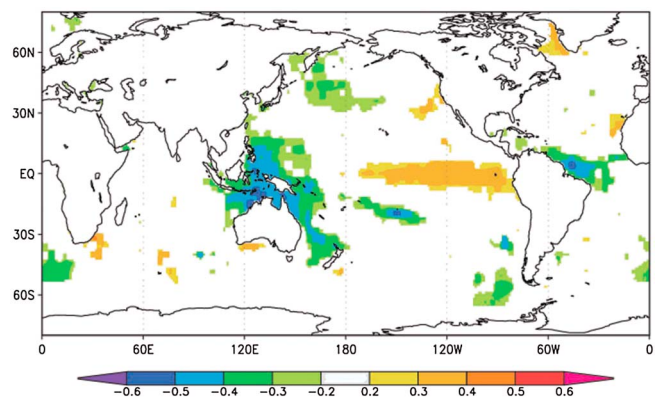

Figure 7. Spatial correlations between the reconstructed OM PDSI for Kinnaur, the western Himalaya, and the SST of the corresponding months (1871–1920). The SSTs over the IPWP/central and eastern Pacific Ocean have a negative/positive correlation with PDSI over the western Himalayan region. The gridded HADISST global ocean surface temperature, monthly 1° area grids from 1870 to present, and the UK Hadley Centre [*Rayner et al.*, 2003] data available on http://climexp.knmi.nl were used in the analyses [*Oldenborgh and Burgers*, 2005].

1920–1960, which coincides with the reduced variability in Pacific SSTs [*Urban et al.*, 2000]. The ENSO teleconnections during this period of reduced interannual variability are known to have weakened considerably over a wide geographical region [*Abram et al.*, 2008; *Yadav* 2011a, 2011b; *Brienen et al.*, 2012].

[11] The OM PDSI was used to investigate the cyclic components using the multitaper method [*Mann and Lees*, 1996]. The time series exhibited significant periodicities of around 2.4, 3.4, 4.8, 8.6–9, and 36–44 years above the 99% significance level. The other periodicities of around 6.4–6.6, 10–10.6, 20–21.8, and 31–33 years exceeded the 95% significance level (Figure 9a). The cycle of 2.3–6.6 years falls in the range of ENSO [*Trenberth*, 1976] and that of 8.6–9 years in the range of the North Atlantic Oscillation mode of variability [*Hurrell and van Loon*, 1997]. The origin of multidecadal
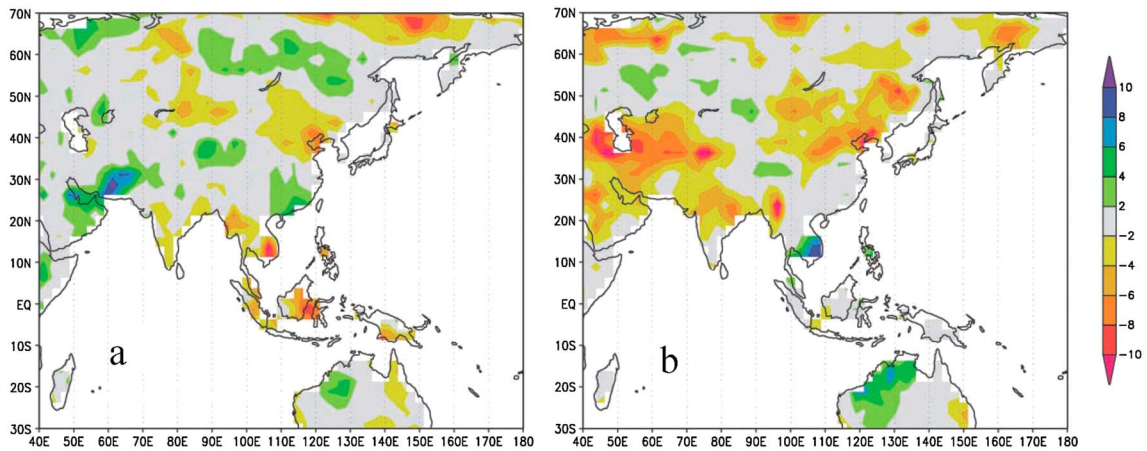
Figure 8. (a) OM precipitation over India and adjacent Asian regions during 1982–1983 (El Niño year). (b) Same as in Figure 8a but for 2000–2001 (La Niña year). The pictures were generated using the KNMI Climate Explorer program [http://climexp.knmi.nl; *Oldenborgh and Burgers*, 2005].
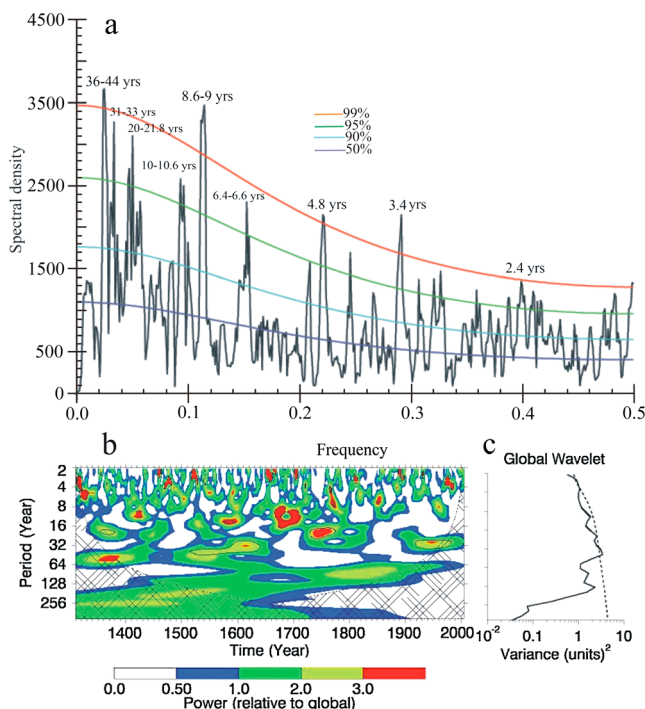
Figure 9. (a) Multitaper power spectra of the reconstructed OM PDSI series (1310–2005). (b) Morlet wavelet spectrum for the full period of PDSI reconstruction (1310–2005 A.D.). Black contours in the power spectrum represent the 95% significance level based on red noise background. The cone-shaped net depicts areas of the spectrum where edge effects become important [*Torrence and Compo*, 1998]. (c) Global wavelet power spectrum. (The wavelet software is available at http://ion.researchsystems.com/cgi-bin/ion-p?page=wavelet.ion&mydata.x=58&mydata.y=36).

oscillation in the range of 36–44 years could be associated with the Atlantic Multidecadal Oscillation (AMO) [*Gray et al.*, 2004; *Knight et al.*, 2005] as well as solar variability [Bruckner cycle; *Raspopov et al.*, 2004]. Interestingly, such multidecadal oscillations have also been reported in the

spring precipitation reconstruction from the western Himalaya [*Yadav*, 2011a] and observational winter precipitation records from northwestern India [*Yadav et al.*, 2012]. To examine the stationarity of low-frequency modes, wavelet analysis [*Torrence and Compo*, 1998] on the full length of OM PDSI reconstruction was performed. The strong frequency components of multidecadal variability at the ~32 to 45 year domain are centered on the sixteenth, early seventeenth, and twentieth centuries (Figure 9b). The modes of such multidecadal components observed in the instrumental and reconstructed precipitation records from the western Himalaya [*Singh et al.*, 2009; *Yadav*, 2011a; *Yadav et al.*, 2012] suggest that long-lasting droughts could be a regular feature in the western Himalaya. It is of significant interest to note here that the wavelet spectrum showing multidecadal variability in the twentieth century is featured by significant energy spread around 1940–1960 when the ENSO-OM PDSI relationship was disrupted. This could possibly suggest the role of AMO in modulating winter droughts over the western Himalaya through the tropical Pacific Ocean. However, more proxy records from the western Himalayan region, similar to those reported here, should be required to substantiate the present findings.

4. Conclusions

[12] A large tree ring data network of Himalayan cedar (nine sites) and Neoza pine (two sites) in Kinnaur, a cold and arid region of Himachal Pradesh in the western Himalaya, was developed. Strong similarity in site and interspecies chronologies revealed common forcing affecting the growth dynamics of the two species growing over a large area. Tree growth over all the sites was found to favorably respond to cool and moist conditions over the extended period from October of the previous year to May of the current year. A reconstruction of seasonalized PDSI for OM using a nested approach was developed back to 1310 A.D. This reconstruction is the first of its kind for the western Himalayan region and provides a window to understand moisture variability in the climate-sensitive western Himalayan region over the past seven centuries.

[13] The OM PDSI reconstruction (1310–2005 A.D.) revealed interannual to multidecadal variations with severe and persistent droughts in the early seventeenth century (1617–1640) and late fifteenth to early sixteenth (1491–1526) centuries. The twentieth century experienced protracted droughts during 1935–1954; however, in terms of severity, these droughts are mild in comparison to the early seventeenth and sixteenth century droughts. The late sixteenth (1561–1590) and early nineteenth (1823–1857) centuries experienced protracted pluvial phases. The early nineteenth century pluvial phase well coincides with the expansion of glaciers in the Himalayas and weakened south Asian summer monsoon. As illustrated by the spatial field correlations with large-scale SSTs, the drought anomalies over the western Himalaya are linked with Indo-Pacific SSTs; however, their relationship is not stationary. We are further improving our tree ring data network for the Himalayan region with the aim of extending the temporal span of the reconstructions to cover the entire millennium. Such data should be useful in understanding the spatiotemporal variability in droughts as envisioned in the MADA [*Cook et al.*, 2010].

References

Abram, N. J., M. K. Gagan, J. E. Cole, W. S. Hantoro, and M. Mudelsee (2008), Recent intensification of tropical climate variability in the Indian Ocean, *Nat. Geosci.*, *1*, 849–853.

Brienen, R. J. W., G. Helle, T. L. Pons, J.-L. Guyot, and M. Gloor (2012), Oxygen isotopes in tree rings are a good proxy for Amazon precipitation and El Nino-Southern Oscillation variability, *PNAS*, doi: 10.1073/pnas.1205977109.

Briffa, K. R., P. D. Jones, T. S. Bartholin, D. Eckstein, F. H. Schweingruber, W. Karlen, P. Zetterberg, and M. Eronen (1992), Fennoscandian summers from AD 500: Temperature changes on short and long timescales, *Clim. Dyn.*, *7*, 111–119, doi: 10.1007/BF00211153.

Cook, E. R., K. J. Anchukaitis, B. M. Buckley, R. D'Arrigo, G. C. Jacoby, and W. E. Wright (2010), Asian Monsoon failure and megadrought during the last Millennium, *Science 328*, 486–489.

Cook, E. R., B. M. Buckley, R. D'Arrigo, and M. J. Peterson (2000), Warm-season temperature since 1600 BC reconstructed from Tasmanian tree rings and their relationship to large-scale sea surface temperature anomalies, *Clim. Dyn.*, *16*, 79–91, doi: 10.1007/s003820050006.

Cook E.R., P. J. Krusic, and P. D. Jones, (2003), Dendroclimatic signals in long tree-ring chronologies from the Himalayas of Nepal, *Int. J. Climatol.*, *23*, 707–732.

Cook, E. R., D. M. Meko, D. W. Stahle, and M. K. Cleaveland (1999), Drought reconstruction for the continental United States, *J. Clim.*, *12*, 1145–1162, doi: 10.1175/1520-0442.

Dai, A., K. E. Trenberth, and T. Qian (2004), A global data set of Palmer Drought Severity Index for 1870-2002: relationship with soil moisture and effects of surface warming, *J. Hydrometeorol.*, *5*, 1117–1130.

Dracup, J.A., K.S. Lee, and E.G. Paulson (1980), On the statistical characteristics of drought events, *J. Water Resources Res.*, *16*, 289–296.

Fagan, B. (2000), The Little Ice Age. Basic Books, New York, 246 pp.

Fritts, H. C. (1976), Tree-rings and Climate. Academic Press, London, 5 67pp.

Gray, S. T., L. J. Graumlich, J. L. Betancourt, and G. T. Pederson (2004), A tree-ring based reconstruction of the Atlantic Multidecadal Oscillation since 1567 A.D., *Geophys. Res. Lett.*, *31*, L12205, doi: 10.1029/2004GL019932.

Himachal Pradesh Development Report (2005), Agriculture pp. 207-224, in Himachal Pradesh Development Report, Planning Commission, Government of India, New Delhi.

Hoerling, M., and A. Kumar (2003), Perfect Ocean for drought, *Science*, *299*, 691–694.

Hughes, M. K. (2001), An improved reconstruction of summer temperature at Srinagar, Kashmir since 1660 AD, based on tree-ring width and maximum latewood density of *Abies pindrow* [Royle] Spach, *Palaeobotanist*, *50*, 13–19.

Hurrell, J.W. and H. van Loon (1997), Decadal variations in climate associated with the North Atlantic Oscillation, *Clim. Change*, *36*, 301–326.

Knight, J. R., R. J. Allan, C. K. Folland, M. Vellinga, and M. E. Mann (2005), A signature of persistent natural thermohaline circulation cycles in observed climate, *Geophys. Res. Lett.*, *32*, L20708, doi:10.1029/2005GL024233.

Mann M. E., and J. M. Lees (1996), Robust estimation of background noise and signal detection in climatic time series, *Clim. Change*, *33*, 409–445.

Martyn, D. (1992), Climate of the World, Elsevier, Amsterdam, 435 pp.

Oldenborgh, G. J., and G. Burgers (2005), Searching for decadal variations in ENSO precipitation teleconnections, *Geophys. Res. Lett.*, *32*, L15701, doi: 10.1029/2005GL023110.

Raspopov, O. M., V. A. Dergachev, and T. Kolstrom (2004), Periodicity of climate conditions and solar variability derived from dendrochronological and other palaeoclimatic data in high latitudes, *Palaeogeogr. Palaeoclimatol. Palaeoecol.*, *209*, 127–139.

Rayner, N., D. Parker, E. Horton, C. Folland, L. Alexander, D. Rowell, E. Kent, and A. Kaplan (2003), Global analyses of sea surface temperature, sea ice, and night marine air temperature since the early nineteenth century, *J. Geophys. Res.*, *108*, 4407, doi: 10.1029/2002JD002670.

Singh, J., and R. R. Yadav (2005), Spring precipitation variations over the western Himalaya, India since AD 1731 as deduced from tree rings, *J. Geophys. Res.*, *110*, D01110, doi: 10.1029/2004JD004855.

Singh J., R. R. Yadav, and M. Wilmking (2009), A 694-year tree-ring based rainfall reconstruction from Himachal Pradesh, India, *Clim. Dyn.*, *33*, 1149–1158.

Sontakke, N. A., N. Singh, and H. N. Singh (2008), Instrumental period of rainfall series of the Indian region [AD 1813-2005]: revised reconstruction, update and analysis, *Holocene*, *18*, 1055–1066.

Torrence, C., and G. P. Compo (1998), A practical guide to wavelet analysis, *Bull. Am. Meteorol. Soc.*, *79*, 61–78.

Trenberth, K. E. (1976), Spatial and temporal variations of the Southern Oscillation, *Quart. J. Roy. Meteorol. Soc.*, *102*, 639–653.

Treydte, K. S., G. H. Schleser, G. Helle, D. C. Frank, V. Winiger, G. H. Haug, and J. Esper (2006), The twentieth century was the wettest period in northern Pakistan over the past millennium, *Nature*, *440*, 1179–1182, doi: 10.1038/nature04743.

Urban, F. E., J. E. Cole, and J. T. Overpeck (2000), Influence of mean climate change on climate variability from a 155-year tropical Pacific coral record, *Nature*, *407*, 989–993.

Yadav, R. R. (2007), Basin specificity of climate change in western Himalaya, India: tree-ring evidences, *Curr. Sci.*, *92*, 1424–1429.

Yadav, R. R. (2011a), Long-term hydroclimatic variability in monsoon shadow zone of western Himalaya, India, *Clim. Dyn.*, *36*, 1453–1462, doi: 10.1007/s00382-010-0800-8.

Yadav, R. R. (2011b), Tree-ring evidence of 20th century precipitation surge in monsoon shadow zone of western Himalaya, *India. J. Geophys. Res.*, *116*, doi: 10.1029/2010JD014647.

Yadav R. R., and W.-K. Park (2000), Precipitation reconstruction using ring width chronology of Himalayan cedar from western Himalaya: preliminary results, *Proc. Ind. Acad. Sci. (Earth Planet. Sci.)*, *109*, 339–345.

Yadav R. R., A. Braeuning, and J. Singh (2011), Tree ring inferred summer temperature variations over the last millennium in western Himalaya, India, *Clim. Dyn.*, *36*, 1545–1554, DOI 10.1007/s00382-009-0719-0.

Yadav, R. K., R. Rupa Kumar, and M. Rajeevan (2012), Characteristic features of winter precipitation and its variability over the northwest India, *J. Earth Syst. Sci.*, *121*, 611–623.